Supporting Information

MOF-Derived Fe-N-C Electrocatalyst via a Dual Ligand Strategy for Efficient Oxygen Reduction in Acidic Media

Yi Sheng,[a] Hongmei Zheng,[a] Jingting Hou,[a] Wanying Zhang,[a] Hong Chen,[a] Luanjie Nie,[b] Jing Zheng,[b] Qingxue Lai[*a]

[a]Jiangsu key Laboratory of Electrochemical Energy Storage Technologies, College of Materials Science and Technologies, Nanjing University of Aeronautics and Astronautics, Nanjing 210016, P. R. China

[b]Department of Chemistry and Materials Science, College of Science, Nanjing Forestry University, Nanjing 210037, P. R. China

*Corresponding authors: laiqingxue@126.com (Q. Lai)

1. Electrochemical Measurements

All catalysts were carried out with a three-electrode system on a CHI760D electrochemical workstation with an MSR electrode rotator (Pine Research Instrumentation) at room temperature. 0.5 M H_2SO_4 solution was prepared as the electrolyte. A graphite rod was employed as the counter electrode while a saturated calomel electrode (SCE) was used as the reference electrode, the potential (E (SCE)) of which was calibrated to reversible hydrogen electrode potential (E (RHE)) using the formula E (RHE) = E (SCE) + 0.24 + 0.0591*pH. The working electrodes were prepared by dispersing 2.0 mg of catalyst into 1.0 ml of Nafion ethanol solution (0.05 wt.%) by sonication for 1 h to acquire the catalyst ink solution which was then dropped on the RDE and the RRDE with the catalyst loading of 0.250 mg/cm^2 for prepared materials, and 0.125 mg/cm^2 for the commercial 30% Pt/C catalyst. The CV tests on RDE were carried out in N_2- or O_2-saturated electrolyte with a scan rate of 10 mV/s and no rotation. LSV tests on RDE and RRDE were carried out with a scan rate of 10 mV/s and a rotation speed of 1600 rpm. The influence of the electric double layer capacitance on the LSV current was eliminated by subtracting the tested curves under N_2-saturated electrolyte from O_2-saturated electrolyte during data processing. The hydrogen peroxide yield and the electron transfer number were calculated from the RRDE LSV data based on the formulas below [Eqs. (1) and (2)]:

$$HO_2^- (\%) = 200 \ \times \ \frac{I_R/N}{I_R/N + I_D} \quad (1)$$

$$n = 4 \ \times \ \frac{I_D}{I_R/N + I_D} \quad (2)$$

Here, I_D and I_R represent the disk current and the ring current respectively, and N is the collection efficiency of the ring disk (0.37). ECSA evaluation: In the N_2-saturation state, the CV test was performed in the non-Faraday interval with different scanning rates from 2 to 25 mV/s. C_{dl} was then calculated via linear fitting of the capacitive $\Delta j/2$ ($\Delta j = j_{positive} - j_{negative}$) at 0.993 V vs. scan rates curve to obtain the slope.

2. Figures and table

Table S1. The Contents of different C structures for S-FeNC, D-FeNC (3:40) and D-FeNC (5:40) from Raman spectra.

sample	T (%)	D (%)	D" (%)	G (%)
S-FeNC	15.06	44.92	15.65	24.37
D-FeNC (3:40)	15.71	43.35	17.90	23.04
D-FeNC (5:40)	15.64	65.61	6.53	18.72
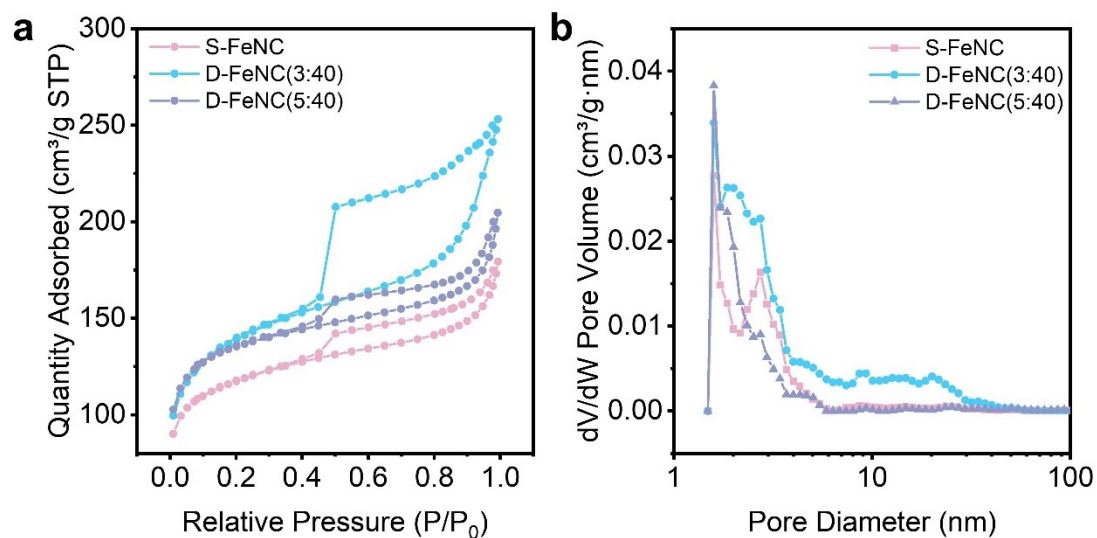
Figure S1. a) N_2 adsorption-desorption isotherm and b) corresponding pore size distribution curve of S-FeNC, D-FeNC (3:40) and D-FeNC (5:40).

Table S2. Comparison of BET specific surface area, micropore specific surface area, total pore volume, pore volume and average pore size.

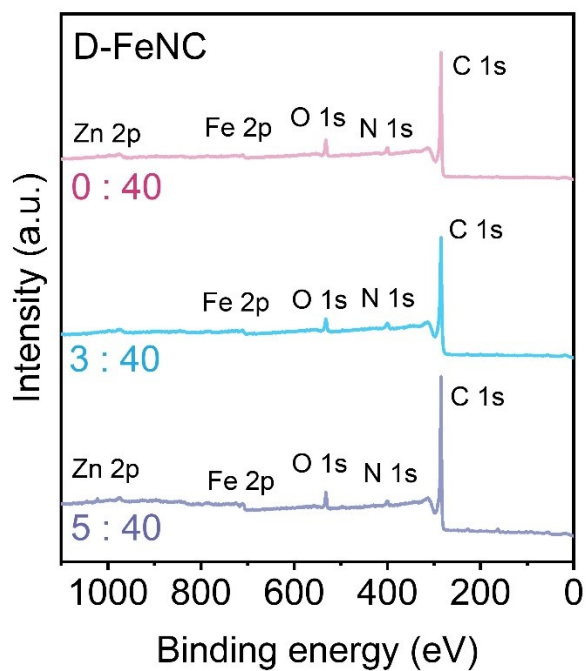| sample	S_{BET}（m^2/g）	S_{Micro}（m^2/g）	V_{total}（cm^3/g）	V_{Micro}（cm^3/g）	D_{avg} (nm)
S-FeNC	437.36	281.82	0.2775	0.1134	4.788
D-FeNC (3:40)	507.90	309.32	0.3915	0.1284	4.639
D-FeNC (5:40)	506.53	373.96	0.3166	0.1513	5.402

Figure S2. XPS spectra of S-FeNC, D-FeNC (3:40) and D-FeNC (5:40).

Table S3. The content of the different carbon species in the high-resolution Fe 2p XPS spectra for S-FeNC, D-FeNC (3:40) and D-FeNC (5:40).

sample	Fe（at.%）	Fe (II) (at.%）	Fe (III) (at.%）
S-FeNC	0.88	0.682	0.198
D-FeNC (3:40)	0.85	0.728	0.122
D-FeNC (5:40)	1.49	1.317	0.173

Table S4. The content of the different carbon species in the high-resolution N 1s XPS spectra for S-FeNC, D-FeNC (3:40) and D-FeNC (5:40).

sample	N1 (%)	N2 (%)	N3 (%)	N4 (%)	N5 (%)	N6 (%)
S-FeNC	12.36	19.8	15.65	22.94	10.69	4.61
D-FeNC (3:40)	23.94	22.95	6.9	27.63	11.05	7.53
D-FeNC (5:40)	8.45	19.9	17.73	29.48	9.32	15.12

Table S5. The content of the different carbon species in the high-resolution C 1s XPS spectra for S-FeNC, D-FeNC (3:40) and D-FeNC (5:40).

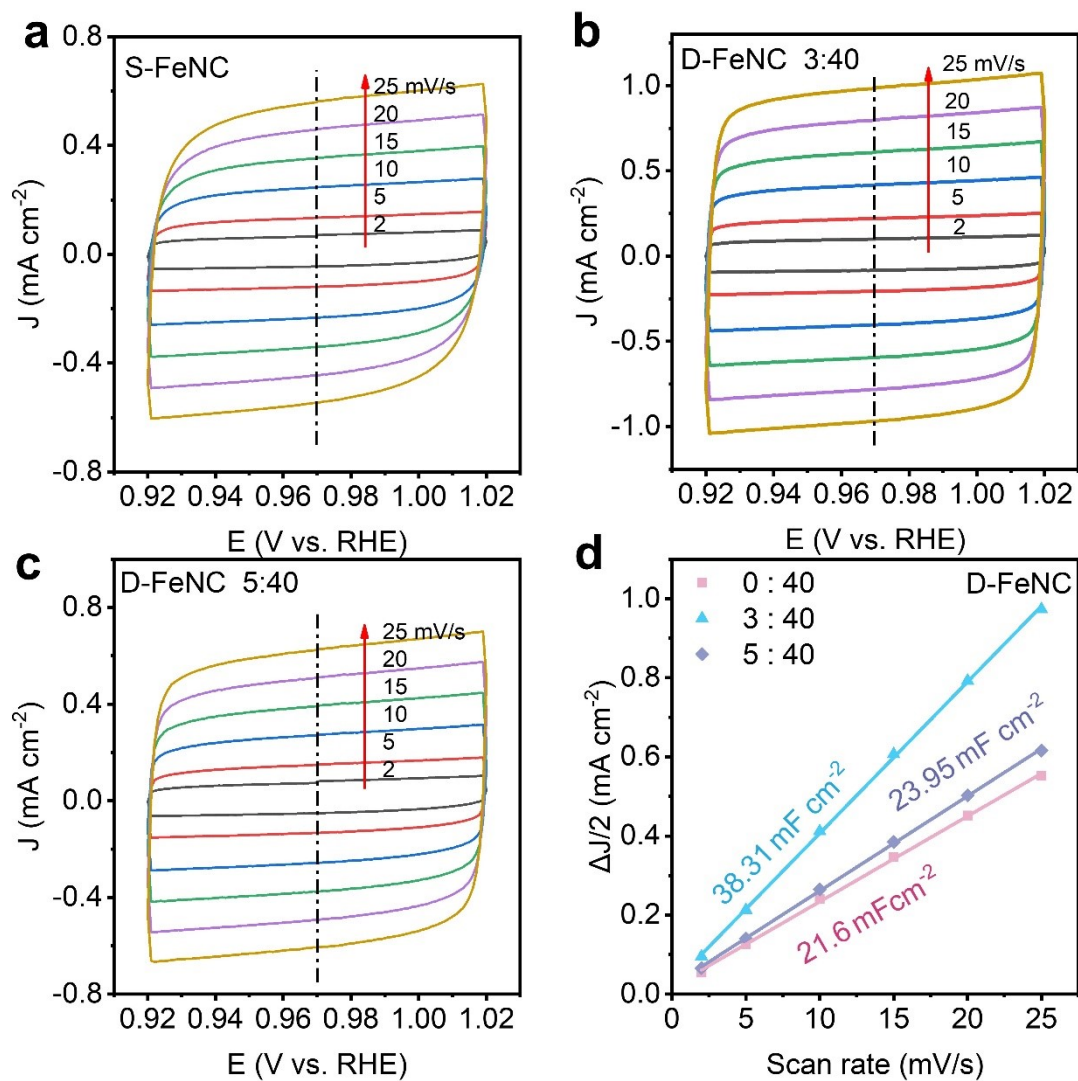| Sample	C1 (%)	C2 (%)	C3 (%)	C4 (%)
S-FeNC	63.95	10.76	11.23	14.06
D-FeNC (3:40)	57.03	16.66	14.80	11.51
D-FeNC (5:40)	61.19	15.74	11.76	11.31

Figure S3. CV curves of a) S-FeNC, b) D-FeNC (3:40), c) D-FeNC (5:40) at different scanning rates. d) comparison of linear fit plots of capacitive Δj/2 vs. scan rates for prepared D-FeNC catalysts with different ligand ratio.
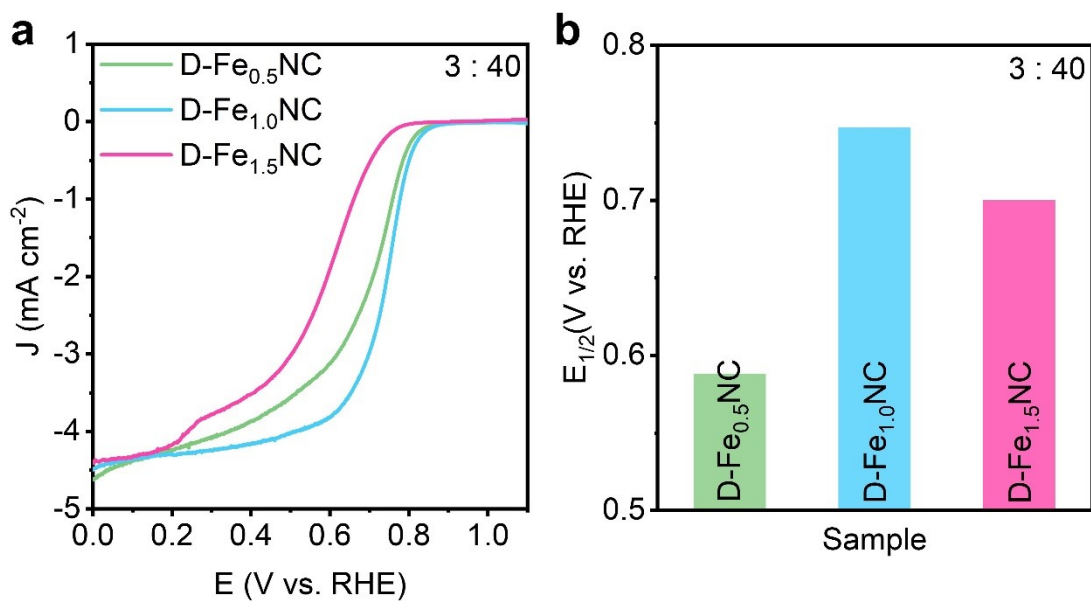
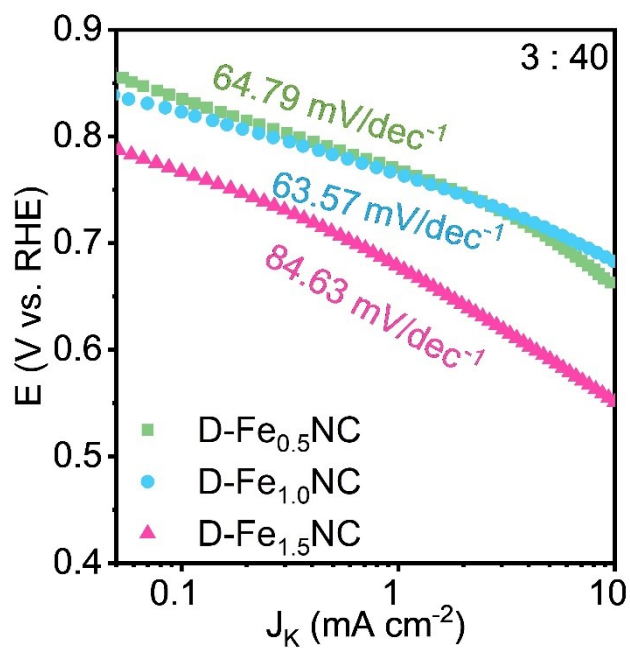**Figure S4.** (a) LSV curves (10 mV/s, 1600 rpm). (b) $E_{1/2}$ for D-Fe$_{0.5}$NC. D-Fe$_{1.0}$NC and D-Fe$_{1.5}$NC.

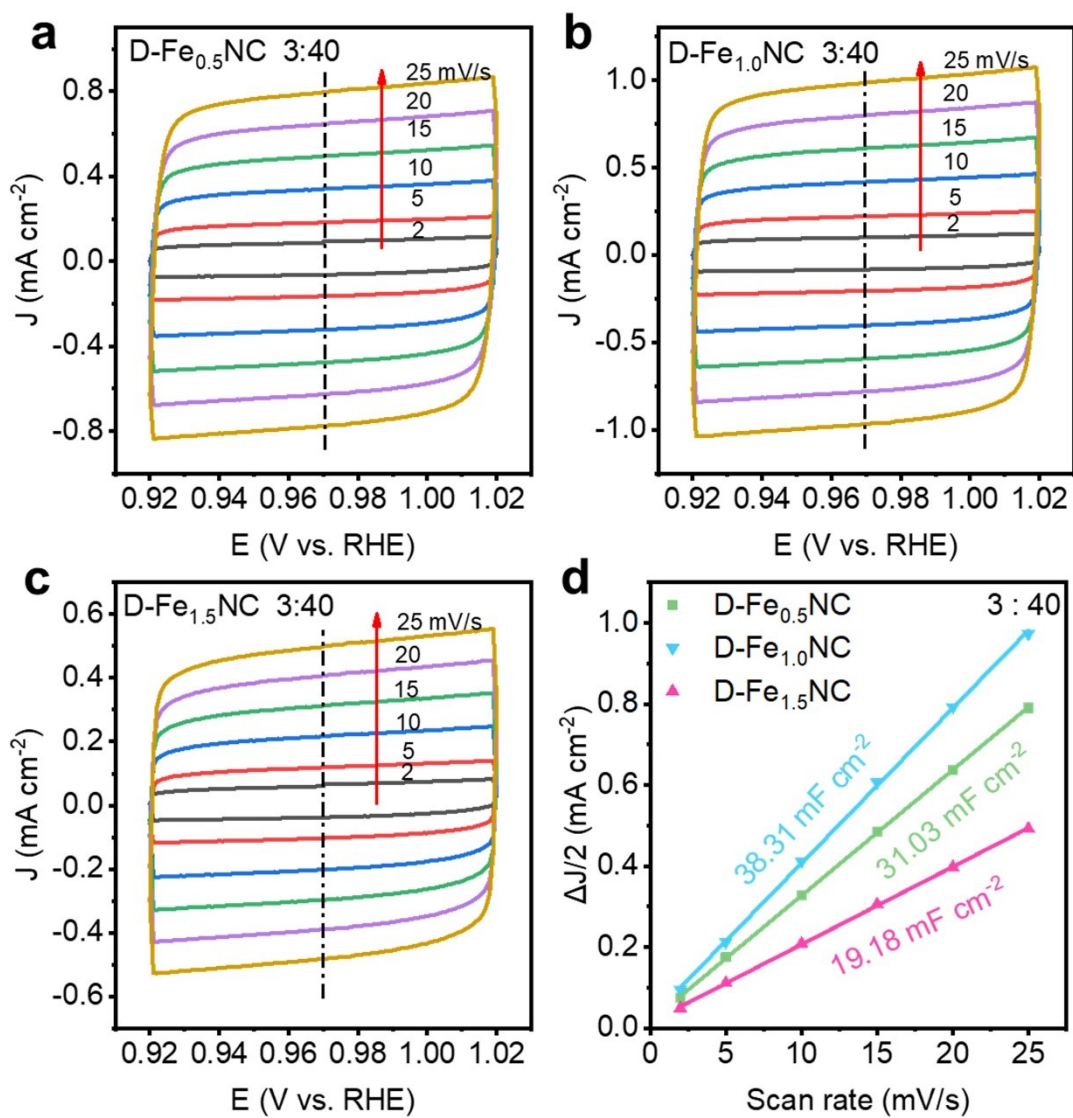**Figure S5.** Tafel plots for D-Fe$_{0.5}$NC. D-Fe$_{1.0}$NC and D-Fe$_{1.5}$NC.

Figure S6. CV curves of a) D-Fe$_{0.5}$NC, b) D-Fe$_{1.0}$NC, c) D-Fe$_{1.5}$NC at different scanning rates. d) comparison of linear fit plots of capacitive Δj/2 vs. scan rates for prepared D-FeNC catalysts with different Zn^{2+}/Fe^{2+} ratio.
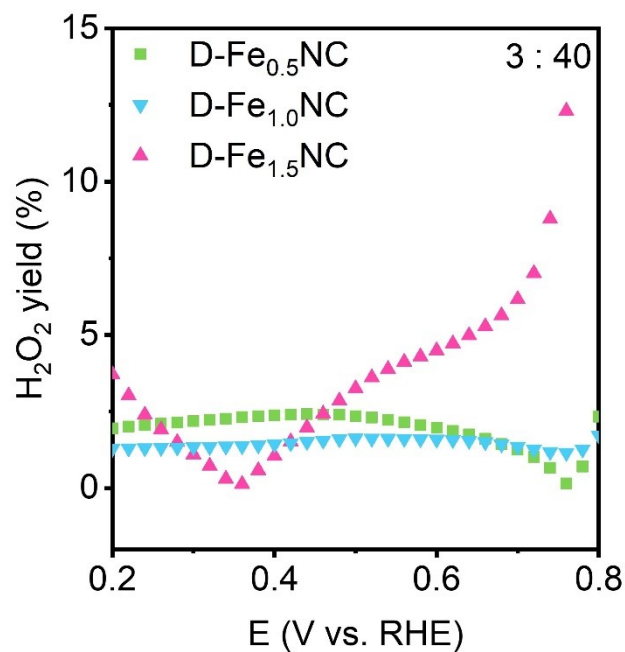
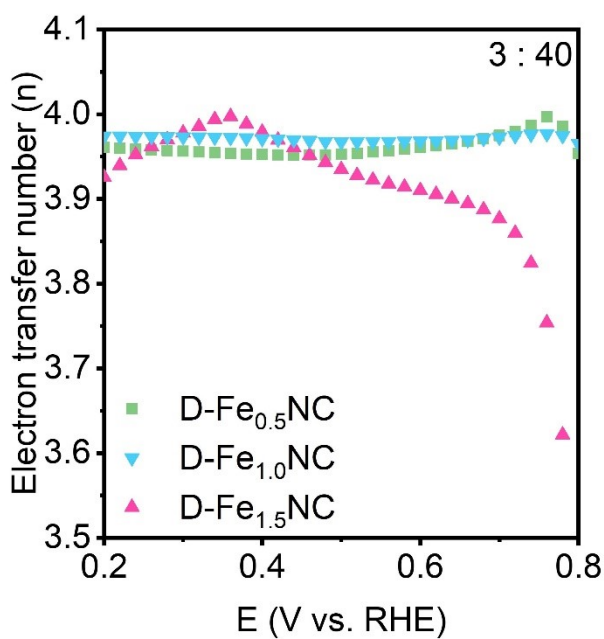**Figure S7.** HO_2^- yield for D-Fe$_{0.5}$NC. D-Fe$_{1.0}$NC and D-Fe$_{1.5}$NC.

Figure S8. electron transfer number (n) D-Fe$_{0.5}$NC. D-Fe$_{1.0}$NC and D-Fe$_{1.5}$NC.